PNC TN941 74−73

The Effects of Bowing Distortions on Heat Transfer in a Seven-Pin Bundle

November, 1974

Power Reactor and Nuclear Fuel Development Corporation

動力炉・核燃料開発事業団 (Power Reactor and Nuclear Fuel Development Corporation)

This paper was first presented to the Session on Heat Transfer in Nuclear Reactor Safety, ASME 1974 Winter Annual Meeting held in New York, N.Y., November 18-22, 1974.

THE EFFECTS OF BOWING DISTORTIONS ON HEAT TRANSFER IN A SEVEN-PIN BUNDLE

by

K. HAGA, Y. DAIGO, A. OHTSUBO and Y. KIKUCHI

Power Reactor and Nuclear Fuel Development Corporation

Oarai, Japan

ABSTRACT

This paper deals with the experimental results of heat transfer in sodium flowing in an electrically heated seven-pin bundle where a pin was bowed to form a point contact. Each pin was 6.5 mm in diameter and had a 450 mm heated length. The bundle was tightly packed with 1.3 mm diameter spacer wires and placed in a hexagonal tube. The pitch-to-diameter ratio (P/D) was 1.22. The central pin was bowed symmetrically near the axial mid-plane to form a point contact with an outer normal pin. The measured temperature rise due to the point contact compared fairly well with the calculation by the PICO code. In addition, experiments were carried out with the normal pin bundle to establish a base case and to evaluate the effect of mixing due to spacer wires. When applied the experimental results to reactor conditions, the temperature rise due to a point contact is considered to be less than 30°K.

NOMENCLATURE

A_{ck} = Free flow area in k-th subchannel, m^2

A_{fsk} = Total frontal area of spacers in k-th subchannel, m^2

b_{jk} = Wetted perimeter between j-th surface and k-th subchannel, m

b_k = Total wetted perimeter of k-th subchannel, m

C_D = Spacer drag coefficient, dimensionless

Cp = Specific heat of sodium, J/(kg-°K)

D = Diameter of heater pin, m

De = 4m = Equivalent hydraulic diameter of flow area, m

d_{ik} = Common perimeter of i-th and k-th subchannel, m

F_1 = Wall shear force, N

F_2 = Spacer drag force, N

F_3 = Interchannel turbulent shear force, N

f_k = Friction factor in k-th subchannel, dimensionless

GA_j = Conductance between j-th surface and ambient enviroment, J/(m-s-°K)

$g(\sigma)$ = Heat transfer coefficient adjusting factor, dimensionless

h = Heat transfer coefficient, $J/(m^2\text{-s-}°K)$

h_k = Heat transfer coefficient in k-th subchannel, $J/(m^2\text{-s-}°K)$

k = Thermal conductivity of sodium, J/(m-s-°K)

K_{jl} = Interface conductance between j-th and l-th surfaces, J/(m-s-°K)

L = Axial length of each subchannel, m

L_e = Length of entrance unheated region, m

L = Distance from bottom end of heated section, m

M = Number of surfaces in problem, dimensionless

m = (cross-sectional flow area)/(wetted perimeter), m

N = Number of subchannels in problem, dimensionless

$Nu = \frac{hDe}{k}$ = Nusselt number, dimensionless

P = Pitch, distance between pin centers, m

Pe = RePr = Peclet number, dimensionless

P_{in} = Inlet pressure, N/m^2

P_{out} = Outlet pressure, N/m^2

Pr = $Cp\mu/k$ = Prandtl number, dimensionless

Q_j = Heat Generation rate at j-th surface, J/(m-s)

q_{AMB_j} = Heat transfer rate to ambient from j-th surface, J/(m-s)

$q_{cond_{jl}}$ = Conduction heat transfer rate from j-th to l-th surface, J/(m-s)
$q_{conv_{jk}}$ = Convection heat transfer rate from j-th surface to k-th subchannel, J/(m-s)
R_e = D $u\rho/\mu$ = Reynolds number, dimensionless
T_a = Temperature of ambient environment, °K
T_b = Bulk temperature, °K
T_i = Temperature in i-th subchannel, °K
T_{in} = Inlet temperature, °K
T_j = Local temperature of j-th surface, °K
T_k = Temperature in k-th subchannel, °K
T_l = Local temperature of l-th surface, °K
T_{out} = Outlet temperature, °K
T_w = Temperature of heating surface, °K
U_i = Average velocity in i-th subchannel, m/s
U_k = Average velocity in k-th subchannel, m/s
u = Flow velocity, m/s
W_k = Flow rate in k-th subchannel, Kg/s
YEDH = Heat eddy diffusivity adjusting factor, dimensionless
YEDM = Momentum eddy diffusivity adjusting factor, dimensionless
ΔT_k = Temperature increase in k-th subchannel, °K
δik = Distance between the nominal centroids of i-th and k-th subchannels, m
εi = Eddy diffusivity in i-th subchannel, m^2/s
εk = Eddy diffusivity in k-th subchannel, m^2/s
θ = Hypothetical contact angle, radian
μ = Viscosity of sodium, Kg/(m-s)
ρ = Density of sodium, Kg/m^3
σ = (distance between displaced and normal pin surfaces)/(distance between normal pin surfaces), dimensionless

INTRODUCTION

In the sodium-cooled fast-breeder reactor, the fuel pins are irradiated by the high neutron flux for a long period and they must endure severe thermal conditions. Although each pin is spaced with a spacer wire or a grid spacer, some pins may possibly bow due to swelling and/or thermal stresses. Extreme bowing may lead to pin contacts. If such a contact occurs, the heat transfer performance near the contact point is degraded resulting in a hot spot, which in turn may cause local boiling or clad melting. It is important from the standpoint of reactor safety to predict the probable magnitude of a hot spot in the event of pin contact.

An experimental study was conducted by R. E. Collingham et al. of the bowing effects on heat transfer in a seven-pin bundle(1). They reported no significant increases in the coolant temperature found beyond 50.8 mm downstream from the contact point.

It is possible, however, that a severe hot spot occurs at a downstream position of less than 50.8 mm, since the coolant flow is stagnant at the downstream region near the contact point. In order to confirm the possibility, authors carried out a more detailed study of the bowing effects on heat transfer in a seven-pin bundle. The experimental results were compared with the calculations by the computer code PICO.

EXPERIMENTAL EQUIPMENT

Loop

The experiments were carried out in the Sodium Boiling and Fuel Failure Propagation Test Loops (SIENA) installed at Oarai Engineering Center, Power Reactor and Nuclear Fuel Development Corporation. These loops are made of mainly type-316 stainless steel and are capable of providing a sodium flow with a maximum inlet sodium temperature of 1023°K, a maximum flow rate of 5×10^{-3} m^3/s, and maximum pressure of 6×10^5 N/m^2.

A schematic diagram of the SIENA loops is shown in Fig. 1. The left side of the SIENA loops is named the SBL loop, containing the T-1 test section for single-pin experiments. The right is the FPL loop and contains the test sections T-2 for 7-pin experiments and T-3 for 37-pin experiments. The main circulation loop of the FPL side, made of schedule-20S piping of 50 mm nominal diameter, comprises a main pump, a main heater, an auxiliary heater, the T-2 test section, an expansion tank, a separator and a main

cooler. The sodium delivered by the main pump enters the T-2 test section after being heated up to the prescribed temperature by the main heater. The sodium leaving the T-2 test section is stored in the expansion tank and the separator and returns to the main pump through the main cooler.

A purification system is installed in the branch of the SBL side. Two cold traps and a plugging indicator control the oxygen concentration in the sodium below 10 ppm. The cover gas is high-purity argon, with combined oxygen and water content held below 5 ppm to prevent contamination of sodium from oxidation.

Test section

Figure 2 shows a sketch of the test section with a bowed pin bundle. Figure 3 is a photograph of the bundle itself. In order to simulate a LMFBR fuel assembly, an electrically heated seven-pin bundle is centered in a hexagonal tube of 24 mm in inner flat-to-flat distance. Each heater pin is 6.5 mm in diameter and is approximately half in length (450 mm heated length and 715 mm gas plenum region) of the Japanese prototype LMFBR MONJU fuel pins. With the exception of the central pin, each pin is wrapped with a 1.3 mm diameter wire clockwise in the flow direction at a 264.8 mm pitch and assembled together into a tight bundle. The distance between pin centers (i.e. the pin pitch) is 7.9 mm and the pitch-to-diameter ratio (P/D) is 1.22.

The central pin is bowed symmetrically over the length of 264.3 mm and the point of maximum bow contacts an outer normal pin at 315 mm above the bottom of the heated section.

A summary of the test section geometry is shown in Table 1.

The sodium enters at the bottom of the test section through an entrance nozzle and flows upward in the bundle. Due to the large length-to-equivalent hydraulic diameter ratio ($L_e/D_e = 40$), the flow develops fully before it enters the heated section.

To keep heat losses to a minimum, the outer wall of the test section is insulated with a compensating heater and a thermal insulator.

Heater pin

The heater pins which were specially made for the present study by Sukegawa Electric Co., Hitachi City, Japan simulate the thermal performance of the MONJU fuel pins. They can be operated at the maximum heat flux of 2.5×10^6 J/(m^2-s) in the flowing sodium of 1173°K.

Each pin consists of a coiled Ta resistor insulated from the swaged stainless steel sheath (0.55 mm thick) by compacted BN. In each pin three thermocouples are embedded in milled grooves. A sketch of a typical heater pin is shown in Fig. 4. All pins are radiographed to check both concentricity and uniformity of the Ta coils. All pins are tested at the heat flux of 2.5×10^6 J/(m^2-s) and at the sodium outlet temperature of 873°K, before they are assembled into a bundle.

Instrumentation

It is important in the present experiment to measure accurately the pin surface temperatures. All the thermocouples which are embedded in the pin, as shown in Fig. 4, were chromel - alumel type and were 0.3 mm in diameter. Their hot junctions are grounded and located at various axial locations.

The local temperatures in the individual coolant channels are measured by 1.3 mm OD chromel-alumel thermocouples, the leads of which form the spacer wires. The inlet and outlet temperatures are measured by 3.2 mm OD thermocouples.

The sodium flow rate is measured by a dc permanent magnetic flowmeter with a calibrational accuracy within 4 %.

The output signals from the thermocouples and flowmeter are recorded on a digital data logging system.

The power to the heater pins is controlled by a variable transformer connected in series with the heater pins, and measured by a precision ammeter - voltmeter, which is calibrated to an accuracy of 2.5 %.

EXPERIMENTAL PROCEDURE

The experiments were conducted to insure that the quantity of dissolved oxides, impurities, and entrained gases were held to a minimum. During

inoperative periods, the loop was purged continuously with high-purity argon. Prior to filling with sodium, the loop was evacuated to an absolute pressure of 10 N/m^2. With the sodium at 473°K, the loop was loaded by pressurizing the dump tank.

All the thermocouples, including pin cladding, inlet and outlet, and individual coolant channels, were calibrated before the experiments and checked periodically during the experiments while the sodium was circulated isothermally at various temperatures.

Prior to making a run, the flow rate was set and the heater pins were adjusted to the fixed power level. Before taking data, sufficient time was allowed to reach steady-state conditions. To verify that the consistency of data was good runs were repeated several times at any one particular set of conditions before going on to the next set. In addition, after proceeding through the complete range of conditions, many repeat runs were made.

The summary of experimental conditions is shown in Table 2.

EXPERIMENTAL RESULTS

Evaluation of heat loss

Before the temperature distributions were measured in the bowed pin bundle, the enthalpy rise was measured between the inlet and outlet of the test section in order to evaluate the heat losses from the test section. The enthalpy rise was evaluated from the measured inlet and outlet temperatures and from the coolant flow rate. Figure 5 compares this fluid enthalpy rise with the electrical heat input. As the agreement is good, the heat losses from the test section were negligible.

Longitudinal wall temperature distribution

Figure 6 shows the measured longitudinal wall (i.e. No.1 pin surface) temperature distribution. The experimental results were compared with the analytical results calculated by the PICO code, whose description is given in the Appendix. In this figure L_h/D_e is the nondimensional distance from the bottom of the heated section. The well temperatures were measured on the surface of the central bowed pin. This figure shows that the wall temperature increases with distance from the bottom of the heated section, and at the point of contact (L_h/D_e = 76.31), the temperature attains a local peak.

The analytical results were calculated by the PICO code under the same conditions that the heat flux was 4.729×10^5 $J/(m^2\text{-}s)$, the flow velocity was 1.96 m/s (equivalent Peclet number of 121), and the inlet temperature of 589°K. The parameter YEDH is the turbulent mixing factor. YEDH = 0 corresponds to no turbulent mixing; the larger the value of YEDH is, the larger the turbulent mixing rate is. The calculated curve for YEDH = 10 agrees fairly better with the measured temperature rise at the contact point.

Circumferential wall temperature distribution

Figure 7 shows the measured circumferential wall temperatures of the outer 6 pins on the cross section 10 mm downstream from the contact point. The experimental results were compared with the analytical results calculated by the PICO code. The thermocouple arrangement to measure the temperature of each outer pin surface is shown in Fig. 7. The experimental conditions are the flow velocity of 1.96 m/s and the heat flux of 4.729×10^5 $J/(m^2\text{-}s)$.

The left portion of the temperature distribution is higher than the right portion. This is due to the directional sweeping crossflow which is created by the spacer wires. In the case of the bowed pin bundle, this sweeping crossflow is disturbed at the gap between the central bowed pin and the outer normal pin (No.7). A counter-clockwise flow does occur due to the spacer wires on the cross section, when viewed from downstream as shown in Fig. 7, and this flow is disturbed by the pin contact. The disturbance of the counter-clockwise flow would have a significant effect on the temperature distribution on the cross section at the contact point. This temperature redistribution is not well described by the PICO code, which cannot treat the sweeping flow due to the spacer wires.

Effect of bowing distortion on heat transfer

Figure 8 shows the observed heat transfer behavior at the point of contact, at 20 mm upstream, and at 10 mm downstream from the point of contact. The wall temperatures were measured on the surface of the central bowed pin facing an outer normal pin (No.7). The bulk coolant temperatures across the cross sections at the same axial positions, where the wall temperatures were measured, were evaluated from the measured inlet and outlet temperatures and from the axial length between the bottom of the heated section and the measuring point. In this figure the experimental results are also shown of a normal seven-pin bundle. It is seen that the Nusselt number is higher with higher Peclet number (i.e. higher flow velocity). The Nusselt number obtained at the contact point is lower than the one in the normal pin bundle, and the difference ratio is about 1/2 for the present experimental range of flow velocities.

If the experimental results are applied to the prototype reactor conditions which are the heat flux of 15×10^5 J/(m^2-s) and the flow velocity of 5 m/s, the temperature rise due to a point contact will be considered to be less than 30°K.

It is more interesting to note that the Nusselt number at 10 mm downstream from the point of contact is lower than that at the point of contact itself. This fact can be attributed to the degraded heat transfer in the stagnant region which is created downstream of the contact point. The front region of the contact point is also a stagnation point of flow, but the heat transfer at this point increases as the flow velocity is made higher. So far as the area of contact is small, the temperature rise at the contact point is not so extreme.

Figure 9 shows the heat transfer behavior obtained on the surface of an outer pin (No.4) (opposite to the contacted outer pin (No.7)) facing toward the central bowed pin 10 mm downstream from the point of contact. In this figure the experimental results are also shown of the central bowed pin at the same axial position. It is seen that the Nusselt number at the outer pin (No.4) is higher than the one at the central bowed pin, and the difference ratio is about 2 for the present experimental range of flow velocities.

CONCLUSIONS

Experimental studies were conducted of the heat transfer in sodium flowing in an electrically heated seven-pin bundle in which a pin was bowed to form a point contact. Experiments were also carried out with the normal pin bundle to establish a base case. Comparison of the experimental results with analytical calculations has yielded the following conclusions.

(1) The measured temperature rise at the contact point agrees fairly well with the calculation by the PICO code. But the circumferential temperature distribution was disturbed by the directional sweeping crossflow due to spacer wires on the cross section 10 mm downstream from the contact point. This temperature redistribution is not well described by the PICO code, which cannot treat the sweeping crossflow.

(2) If the experimental results are applied to the reactor conditions, which are the heat flux of 15×10^5 J/(m^2-s) and the flow velocity of 5 m/s, the temperature rise due to a point contact is estimated to be less than 30°K.

ACKNOWLEDGEMENT

The authors wish to express their thanks to Mr. O. Kawaguchi and Mr. M.Hori, Power Reactor and Nuclear Fuel Development Corporation, for their valuable suggestions and discussions throughout the performance of the present study. The authors are in debted to the assistance of Mr. T. Kariya and Mr. T. Okouchi who contributed to the accomplishment of the experiments.

REFERENCES

1. Collingham, R. E., Yatabe, J. M., Hill, V. R. and Thorne, W. L., "Experimental Temperature Distributions in Liquid Metal Fast Breeder Reactor Fuel Assemblies, the Effect of Bowing

Distortions,"HEDL-TME 72-23, February, 1972.

2. Kattchee, N. and Reynolds, W.C., "ARMY GAS-COOLED REACTOR SYSTEMS PROGRAM, HECTIC-II, AN IBM 7090 FORTRAN COMPUTER PROGRAM FOR HEAT TRANSFER ANALYSIS OF GAS OR LIQUID COOLED REACTOR PASSAGES," AEC Research and Development Report, Report No. IDO-28595, December, 1962.

3. Yu, W. S. and Dwyer, O. E., "Heat Transfer to Liquid Metals Flowing Turbulently in Eccentric Annuli-II," Nucl. Sci. Eng., 27, 1-9 (1967).

APPENDIX: THE PICO CODE

Introduction

There are a number of computer programs for thermal-hydraulic subchannel analysis of fuel pin bundles. These codes, however, cannot treat thermal bowing of fuel pins. A computer code PICO was developed to estimate temperature distributions in the event of pin contact due to the extreme bowing.

The PICO code is a revised version of HECTIC-II[2] which is a computer program for calculating pressure drop, flow rates, heat transfer rates, and temperature in heat exchangers such as fuel elements of typical gas- or liquid-cooled nuclear reactors. The original HECTIC-II code cannot treat the change of geometry in the axial direction. The PICO code, however, considers a special subchannel between a bowed pin and a normal pin. When the area of this subchannel is zero, the bowed pin contacts the normal pin.

The interactions between adjacent subchannels are due to turbulent interchange, pressure induced diversion crossflow, and transverse thermal conduction. The directional sweeping crossflow due to spacer wires is not considered here.

PICO was written specifically for the geometry of the seven-pin bundle but it can easily be extended to larger bundles with different internal configurations.

Geometries

Figure 10 shows a half sector of the 7-pin bundle, in which it is assumed that the central No.1 pin is bowed to contact the outer No.7 pin. The flow area is divided into 7 subchannels as shown in Fig. 10. The central No.7 subchannel, which is especially considered to calculate the temperature rise due to the bowed pin, is surrounded by the bowed pin, the normal pin and No.1 subchannel. The circumferential heating length of each pin for this subchannel is θD, where θ is a hypothetical contact angle.

Figure 11 shows the axial cross section of the bundle. Each pin and each subchannel are divided into many axial nodes. During this process the bowed pin is transformed to a series of uniformly displaced short pins. At the contact node the flow area of the No.7 subchannel is assumed to be zero. The flow and temperature calculations are carried out step by step from upstream in axial direction.

Fluid flow calculations

PICO divides the total flow through N prescribed subchannels in such a manner that pressure drops through all subchannels are identical. The effects of wall friction, drag against spacers, and turbulent eddy exchange between subchannels are calculated. But the sweeping flow due to spacer wires is not considered in this code.

The equation for pressure drop in each subchannel is obtained from a momentum analysis on the fluid in a flow tube. Thus by balancing the forces which act upon the fluid in the k-th subchannel at an axial node, one obtains the following expressions:

$$A_{ck}(P_{in}-P_{out}) = F_1(\text{wall shear force}) + F_2(\text{spacer drag force}) + F_3(\text{interchannel turbulent shear force}) \quad (1)$$

where

$$F_1 = \frac{\rho U_k^2}{2} \cdot f_k b_k L \quad (2a)$$

$$F_2 = A_{fsk} \cdot \frac{\rho U_k^2}{2} \cdot C_D \quad (2b)$$

$$F_3 = \sum_{i=1}^{N} YEDM.\rho. \frac{\epsilon i+\epsilon k}{2} \cdot \frac{U_k-U_i}{\delta ik} \cdot d_{ik}L \quad (2c)$$

Heat transfer calculations

The heat transfer calculations for PICO involve three basic heat transfer modes: 1) surface-to-coolant convection, 2) intersurface conduction and 3) surface to environment heat loss.

Surface-to-coolant convection. A heat transfer coefficient adjusting factor $g(\sigma)$ is considered to calculate the effect of pin contact conditions, where σ represents the magnitude of the displacement and is a ratio of the distance between displaced and normal pin surfaces to the distance between normal pin surfaces. The values of $g(\sigma)$ were adapted from the results published by Yu and Dwyer[3] as follows:

$$\text{for } \sigma = 1.0\sim0.7 \quad g(\sigma)=\frac{5.7-14.7\sigma+10\sigma^2}{5.55-14.1\sigma+9.55\sigma^2}$$
$$\sigma = 0.7\sim0.3 \quad g(\sigma)=0.838 \qquad (3)$$
$$\sigma = 0.3\sim0.0 \quad g(\sigma)=2.79\sigma$$

The local surface-to-coolant convection heat transfer rate per unit length from the j-th surface to the k-th subchannel is

$$q_{conv_{jk}} = q(\sigma_k)h_k b_{jk}(T_j-T_k) \qquad (4)$$

Intersurface conduction. The heat conduction rate per unit length from the j-th to the l-th surface is given by

$$q_{cond_{jl}} = K_{jl}\cdot(T_j-T_l) \qquad (5)$$

Surface-to-environment heat loss. The heat transfer rate per unit length from the j-th surface to ambient is given by

$$q_{AMB_j} = GA_j\cdot(T_j-T_a) \qquad (6)$$

Any of the surface-to-environment heat loss will be zero in most problems.

Temperature calculations

For steady-state conditions, the heat generation per unit length at the j-th surface must be equal to the heat transferred by all considered modes, thus:

$$Q_j = \sum_{k=1}^{N} q_{conv_{jk}} + \sum_{l=1}^{M} q_{cond_{jl}} + q_{AMB_j} \qquad (7)$$

An energy balance on a node of the k-th subchannel is given by the following equation:

$$W_k C_p \frac{\Delta T_k}{L} = \sum_{j=1}^{M} g(\sigma_k)h_k b_{jk}(T_j-T_k)$$
$$+YEDH\cdot\rho C_p \sum_{i=1}^{N} \frac{\varepsilon_i+\varepsilon_k}{2}\cdot\frac{T_k-T_i}{\delta_{ik}} d_{ik} \qquad (8)$$

Table 1 Summary of test section geometry

Number of heater pins in bundle	7
Diameter of heater pin, mm	6.5
Pitch, distance between heater pin centers, mm	7.9
Pitch-to-diameter ratio	1.22
Length of heater pins, mm	1555
Length of entrance unheated region, mm	175
Heated length, mm	450
Geometrical arrangement	Equilateral triangular
Spacers of heater pins	Spiral wire (clockwise direction)
Diameter of spacers, mm	1.3
Pitch of spacer, mm	264.8
Inner flat-to-flat distance of hexagonal tube, mm	24

Table 2 Summary of experimental conditions

Sodium temperature range, °K	580 to 667
Heat flux range, $J/(m^2-s)$	0.75×10^5 to 5.44×10^5
Flow velocity range, m/s	0.28 to 5.13
Reynolds number range	3634 to 64200
Prandtl number range	0.00576 to 0.00503
Peclet number range	17.3 to 320
Flow direction	Vertically upward

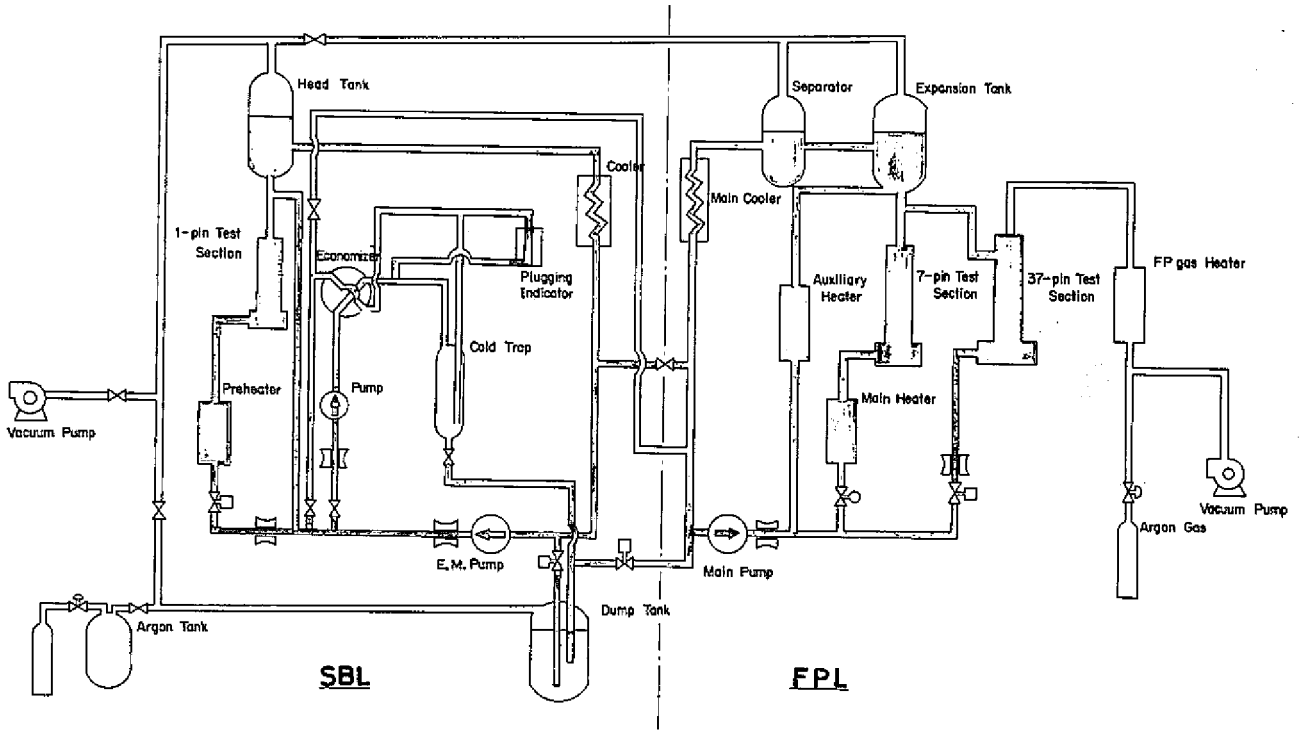

Fig.1 Schematic diagram of sodium boiling and fuel failure propagation test loops SIENA

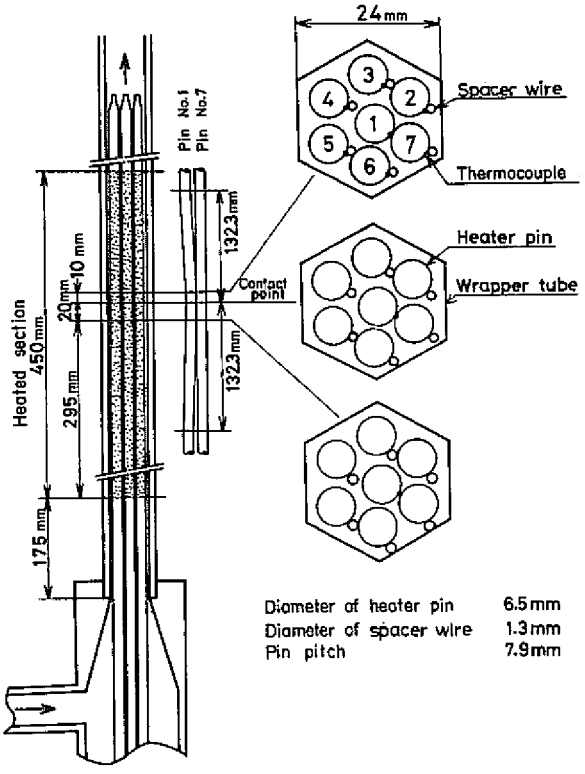

Fig.2 Test section with a bowed pin bundle

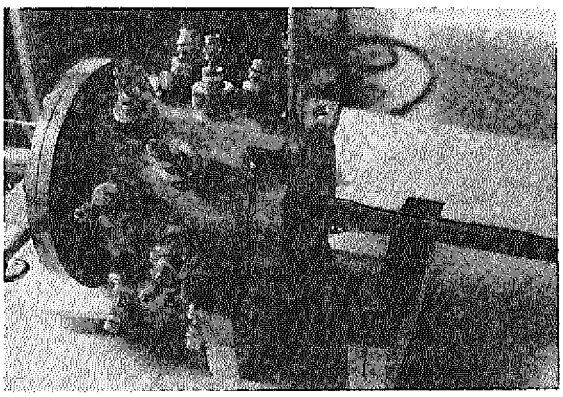

Fig.3 Photograph of a bundle assembly

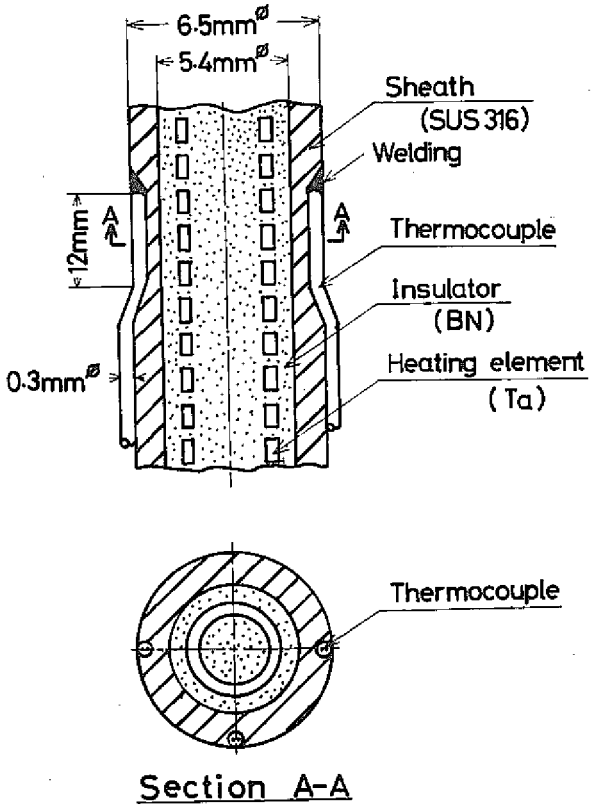

Fig.4 Sketch of a typical heater pin

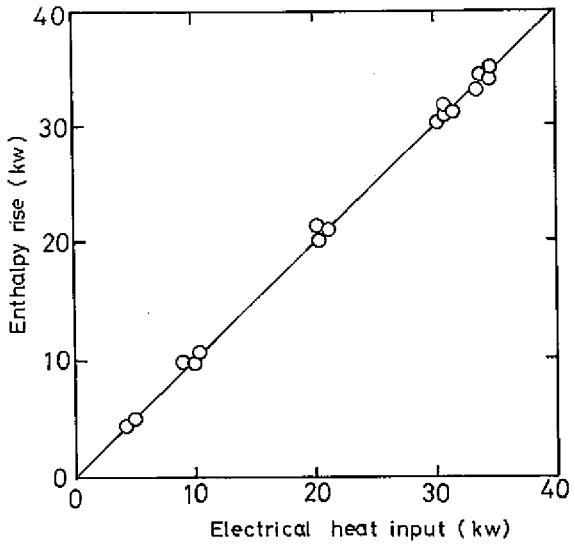

Fig.5 Relation between electrical heat input and fluid enthalpy rise

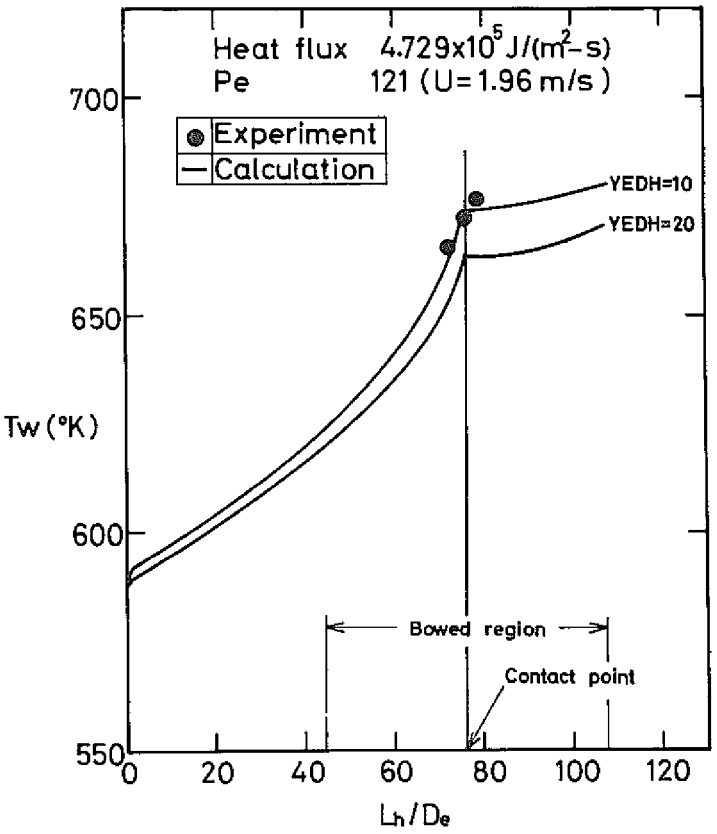

Fig.6 Longitudinal wall temperature distribution

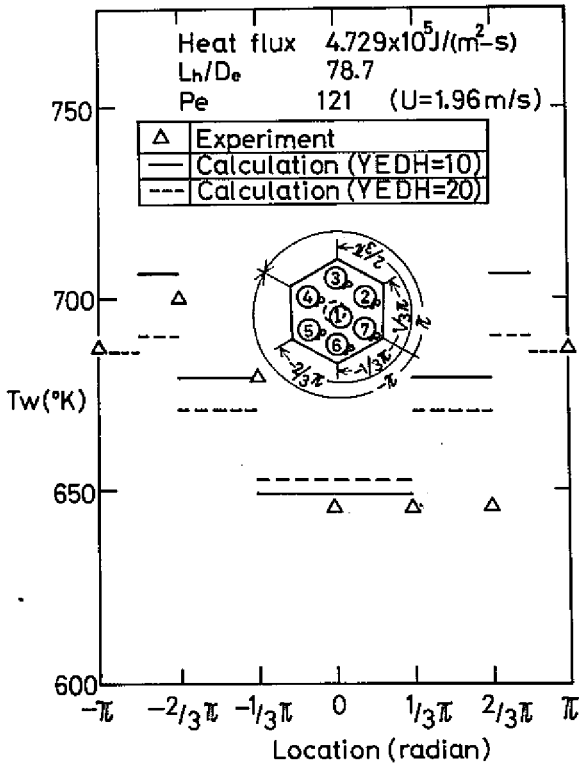

Fig.7 Circumferential wall temperature distribution 10 mm downstream from the contact point

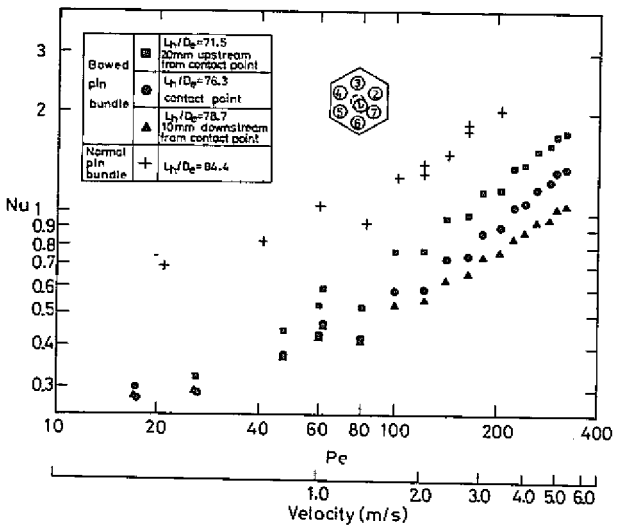

Fig.8 Heat transfer behavior near the contact point; central bowed pin (No.1)

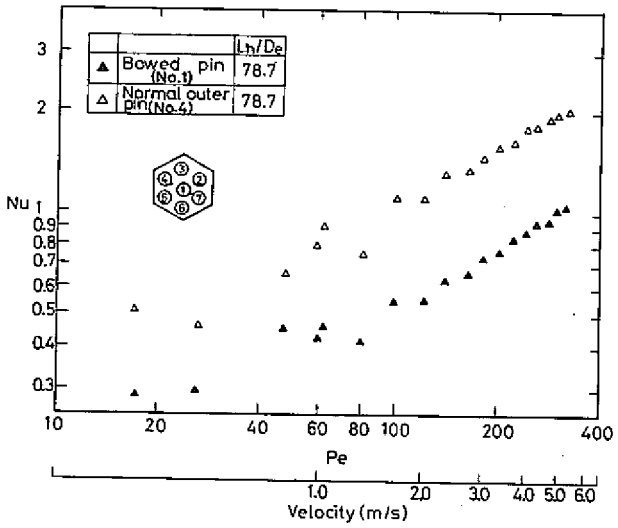

Fig.9 Heat transfer behavior 10 mm downstream from the contact point; central bowed pin (No.1) and outer normal pin (No.4)

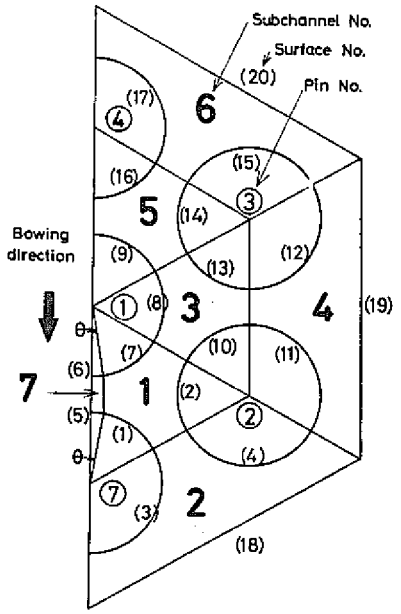

Fig.10 Radial cross section of a 7-pin bundle geometry for the PICO code

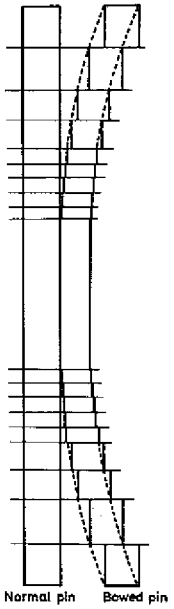

Fig.11 Axial cross section of a transformed bowed pin bundle for the PICO code